Available online at www.sciencedirect.com
ScienceDirect
Journal of Photochemistry and Photobiology A: Chemistry 183 (2006) 322–328
Journal of Photochemistry and Photobiology A:Chemistry
www.elsevier.com/locate/jphotochem

Correlated measurements of plasmon resonance Rayleigh scattering and surface-enhanced resonance Raman scattering using a dark-field microspectroscopic system

Tamitake Itoh [a,b,*], Yasuo Kikkawa [a], Kenichi Yoshida [a], Kazuhiro Hashimoto [a], Vasudevanpillai Biju [b], Mitsuru Ishikawa [b], Yukihiro Ozaki [a]

[a] *Department of Chemistry, School of Science and Technology, Kwansei Gakuin University, Sanda, Hyogo 669-1337, Japan*
[b] *Nano-Bioanalysis Team, Health Technology Research Center, National Institute of Advanced Industrial Science and Technology (AIST), 2217-14 Hayashi-cho, Takamatsu, Kagawa 761-0395, Japan*

Available online 5 July 2006

Abstract

The current work demonstrates development of a dark-field microspectroscopic system by combining Rayleigh scattering spectroscopy and surface-enhanced resonance Raman scattering (SERRS) spectroscopy on an optical microscope. The microspectroscopic system was helpful for identifying plasmon resonance Rayleigh scattering from isolated Ag nanoaggregates and simultaneous measurements of SERRS signals from the nanoaggregates. Furthermore, the use of a microspectroscopic system for correlated measurements of plasmon resonance Rayleigh scattering and SERRS signals enabled us to establish relationships between SERRS, excitation polarization, excitation energy, and plasmon resonance energy. The relationships between SERRS, excitation polarization, excitation energy, and plasmon resonance energy allowed us not only to identify optimum excitation condition for maximum SERRS but also clarification of a mechanism underlying SERRS. Details of microspectroscopic system, measurement of plasmon resonance Rayleigh scattering and SERRS, and a mechanism of SERRS are discussed.

Keywords: SERRS; Rayleigh scattering; Plasmon resonance; Ag nanoaggregate; Dark-field microspectroscopy; Single nanoparticle spectroscopy

1. Introduction

Noble metal nanoparticles (NPs) exhibit strong optical resonance in the near UV to NIR region. This resonance is attributed to particle plasmon due to collective oscillations of conduction band electrons in NPs [1]. Under photoexcitation the particle plasmon couple to the excitation light and produces huge enhancement of electromagnetic (EM) field in metal NPs [1–6]. The enhanced EM field is widely useful for analytical and spectroscopic characterization of different chemical structures, and physical and chemical processes under a broad terminology of "surface-enhanced spectroscopy". Based on the type of interaction between a molecule/system and the enhanced EM field, surface-enhanced spectroscopy has been classified into surface-enhanced fluorescence [7], surface-enhanced Rayleigh scattering [8], surface-enhanced absorption [9], surface-enhanced Raman scattering [2–5,10–19], and surface-enhanced nonlinear emission [20]. Surface-enhanced resonance Raman scattering (SERRS) is specifically attractive due to enormous enhancement of SERRS signal by a factor of 10^8 to 10^{14}. The huge enhancement factor involved in SERRS lifted detection limit of molecules from ensemble to single-molecule level [3–5,11–18].

In recent experimental and theoretical investigations the origin of SERRS enhancement was discussed in terms of coupling between EM field and plasmon of metal nanoaggregates [2–6,10–19]. Contribution of a chemical enhancement to the SERRS signal is also possible [10,21]. From investigations using atomic force microscopy (AFM) and scanning electronic microscopy (SEM) it has been identified that the SERRS enhancement is related to NP junctions in aggregates [4,5,12,13,18]. Also, recent calculations of EM field at interparticle junctions in metal nanoaggregates supported enormous enhancement of SERRS by coupling to plasmon resonance [3–6]. Therefore, characterization of relationships between SERRS and plasmon resonance of metal nanoaggregates would be helpful for identifying ideal conditions for SERRS measure-

* Corresponding author. Tel.: +81 87 869 3557; fax: +81 87 869 4113.
E-mail address: tamitake-itou@aist.go.jp (T. Itoh).

1010-6030/$ – see front matter © 2006 Elsevier B.V. All rights reserved.
doi:10.1016/j.jphotochem.2006.06.031

ments. Nonetheless, experimental investigations of relationships between SERRS and plasmon resonance are difficult due to size and shape dependencies of the plasmon resonance energy of metal nanoaggregates [2,10,16]. Therefore, plasmon resonance bands become averaged in collective ensemble measurements and the relationships are difficult to be discusses due to inhomogeneous broadening of plasmon resonance bands. The difficulties associated with ensemble averaging were circumvent by developing a dark-field microspectroscopic system for correlated measurements of plasmon resonance and SERRS.

In the current work, we discuss details of a new microspectroscopic system which allowed simultaneous measurements of plasmon resonance Rayleigh scattering spectra and SERRS spectra from single-Ag nanoaggregates, and a direct demonstration of relationships between plasmon resonance and SERRS. Specifically, we have identified three kinds of relationships among excitation polarization, excitation energy, and plasmon resonance energy. The microspectroscopic system and the correlated spectral measurements would be important to identify optimum condition of SERRS detection and to investigate mechanistic details of SERRS.

2. Experimental

2.1. Preparation of SERRS-active Ag nanoaggregates

Colloidal solutions of Ag NPs were prepared following a literature method [22]. Steps involved in the preparation of samples for spectromicroscopic analyses are summarized here. An aqueous solution of a mixture of NaCl (10 mM) and rhodamine 6G (R6G, 6.4×10^{-9} M) was added to a colloidal solution (9.6×10^{-11} M) of Ag NPs. This mixture was incubated for 5 min at room temperature and spin coated on a slide glass. From correlated plasmon imaging and scanning electron microscopy (SEM) imaging we identified that SERRS-active Ag nanoaggregates are composed of several Ag NPs of ~40 nm diameter. The Ag nanoaggregates were covered using a thin layer of a NaCl (3.5 M) aqueous solution for obtaining stabilized SERRS signals as shown in Fig. 1 [16,17].

2.2. Microspectroscopy setup for detecting plasmon resonance Rayleigh scattering signals

The experimental setup for measuring Rayleigh scattering spectra of single-Ag nanoaggregates is shown in Fig. 1. In an inverted optical microscope (Olympus IX70), a collimated unpolarized white light beam from a 100 W halogen lamp was introduced into a sample surface through a dark-field condenser lens. Rayleigh scattering light from a single bright spot, likely a single-Ag nanoaggregate, was collected using an objective lens O1 (LCPlanFl, 60×, N.A. 0.7, Olympus, Tokyo) and detected using either a digital camera (CCD1) (Nikon, COOLPIX5000, Tokyo) for plasmon and SERRS imaging or a polychromator (Pro-275, Acton, Tokyo) connected to a charge-coupled device (CCD2) (DV434-FI, Andor, Tokyo) for spectral measurements. We detected Rayleigh scattering light from a single-Ag nanoaggregate and minimized background Rayleigh scattering light by

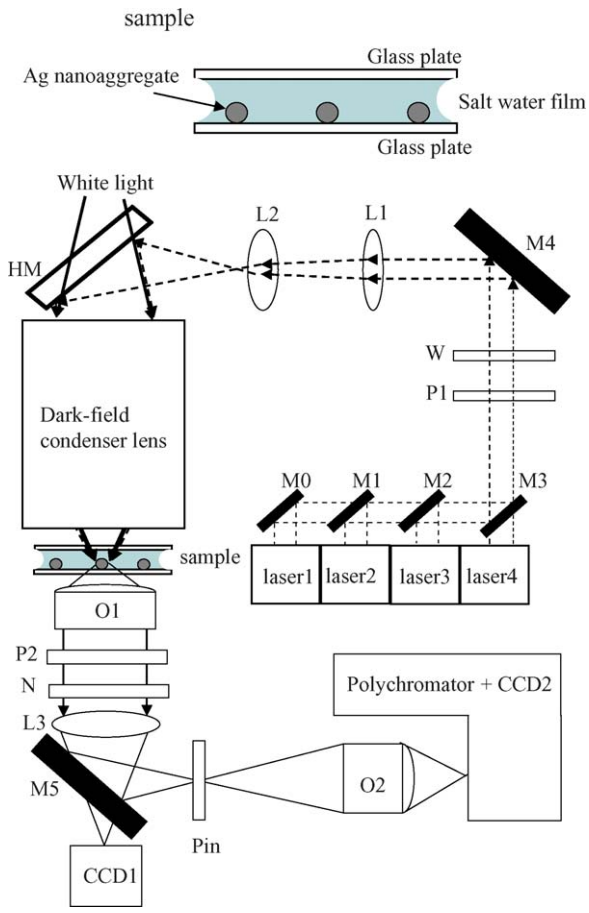

Fig. 1. Microspectroscopy setup for simultaneous measurement of SERRS and plasmon resonance Rayleigh scattering from single-Ag nanoaggregates. An aqueous solution of NaCl and Ag nanoaggregates adsorbed with R6G were sandwiched between two glass plates. M0–M5 are mirrors; P1 and P2 are polarizers; W is a 1/4 wave-plate; L1–L3 are convex lenses; HM is a half mirror; O1 and O2 are objective lenses; N is a notch filter; Pin is a pinhole; CCD1 and CCD2 are charge-coupled devices.

selective measurement on a sample area of 1.5 μm diameter (shown in an open circle in Fig. 2A) using a pinhole (300 μm radius) set in the image plane of the inverted microscope [23]. The white light spectral shape of the 100 W halogen lamp was compensated by normalizing the Rayleigh scattered light intensity using Rayleigh scattering from a frost plate (DFQ1-30C02-240, SIGMA, Tokyo); the frost plate was found to have uniform Rayleigh scattering efficiency within the detection range of the spectrometer.

2.3. Microspectroscopic setup for detecting SERRS signals

The experimental setup for SERRS spectral measurement of single-Ag nanoaggregates is shown in Fig. 1. The inverted optical microscope was common to detections of Rayleigh scattering and SERRS signals. Excitation lasers used were an Ar ion laser (L1) (2016-05, Spectra Physics, Tokyo), second harmonics (532 nm) of a LD YAG laser (L2), a Kr ion laser (L3) (643R-AP-A01, Melles Griot, Tokyo), and a He–Ne laser (L4) (05-LHP-151, Melles Griot, Tokyo). A set of mirrors (M1

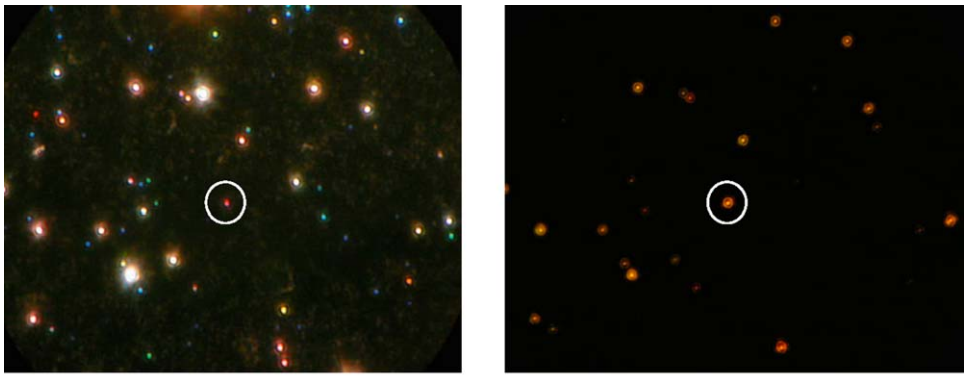

Fig. 2. Plasmon resonance Rayleigh scattering (A) and SERRS (B) images of Ag nanoaggregates dispersed on a glass plate. White circles in (A) and (B) correspond to areas selected by a pinhole shown in Fig. 1.

to M3) on position controlled ports were used for selecting 457, 488, 514, 532, 567, and 633 nm laser wavelengths for SERRS excitations. The laser beams were passed through a polarizer (P1) and a quarter-wave plate (W) and reflected by a half mirror (HM) into the dark-field condenser lens before focusing at the sample surface. We adjusted the focal point of the laser beams to that of white light by using two convex lenses (L1 and L2). This arrangement was helpful for simple detection of both the Rayleigh scattering and SERRS signals without additional optics. SERRS signal from a single bright spot (Fig. 2B) was collected using the common objective lens (O1), passed through a holographic notch filter (N) [HNF–(457.8, 488, 514, 3, 532, 568.2, and 632.8)–1.0, Kaiser Optic Systems Inc., Ann Arbor], and detected using the CCD cameras in the same way as Rayleigh scattering detection. The excitation laser power was 100 mW/cm^2 at the sample surface. We selected SERRS signal from single-Ag nanoaggregates and minimized the contribution of background fluorescence to SERRS by using a pinhole. The pinhole allowed us selective measurements of SERRS signals from a small sample area of 1.5 μm diameter.

2.4. Polarization dependence of plasmon resonance Rayleigh scattering and SERRS

Polarization dependence of Rayleigh scattering spectra and SERRS spectra from single-Ag nanoaggregates were measured under unpolarized white-light excitation and circularly polarized laser excitation, respectively. Polarization dependence of plasmon resonance Rayleigh scattering and SERRS were detected from polarization of scattered light. Polarization dependence was measured by rotating a common polarization plate (P2). The use of a common polarization plate was useful for comparing polarization dependence of Rayleigh scattering spectra and SERRS spectra without polarization-angle error [14]. Polarization dependence is related to intrinsic anisotropy of an optical system and we detected the intrinsic anisotropy from polarization dependence of unpolarized transmitted light. Polarization-angle was arbitrarily considered to be parallel and perpendicular to a grating inside the polychromator. From the transmittance (100:95) of light in the parallel and perpendicular directions we concluded that the intrinsic polarization dependence of the microspectroscopic system is negligible.

3. Results and discussion

3.1. Excitation polarization dependence of SERRS

In order to understand optical correlation between excitation polarization and SERRS we investigated polarization dependence of plasmon resonance Rayleigh scattering and SERRS of single-Ag nanoaggregates. For this, we calculated both the optical far-field corresponding to Rayleigh scattering spectrum and the near-field of an Ag nanoaggregate in which two nanoparticles (diameter ∼20 nm) are in contact. This two-NP system is one of the simple SERRS-active systems [4,5,11–18]. For the calculation we used a finite difference time domain (FDTD) method (PLANC-FDTD Ver. 6.2, Information and Mathematical Science Laboratory Inc., Tokyo). In the current work we compared polarization dependence among the calculated Rayleigh scattering spectra, experimental Rayleigh scattering spectra, and SERRS of a Ag nanoaggregate.

The calculated far-field spectra are shown in Fig. 3A. When the incident light polarization was parallel to the long axis of a nanoaggregate the Rayleigh scattering spectra showed two distinctive plasmon resonances centered at 355 and 630 nm. On the other hand, only one plasmon resonance centered at 350 nm was significant when the polarization of incident light was perpendicular to the long axis of the nanoaggregate. Calculated near-field images corresponding to 350 and 630 nm laser excitations with excitation polarizations perpendicular and parallel to the long axis of Ag nanoaggregate are shown in Fig. 3B. The color gradient in the calculated images are proportional to SERRS EM enhancement factor which is defined as 4th power of the ratio of incident EM field (E_{in}) and enhanced EM field (E_{loc}); $|E_{loc}/E_{in}|^4$ [3,4]. When the excitation polarization was parallel to the long axis an enhanced near-field was observed at a particle junction; on the other hand, enhancement was negligible when the excitation polarization was perpendicular to the long axis. The polarization-angle dependence of the plasmon resonance band at 630 nm (Fig. 3A) was well fitted with a $\cos^2\theta$

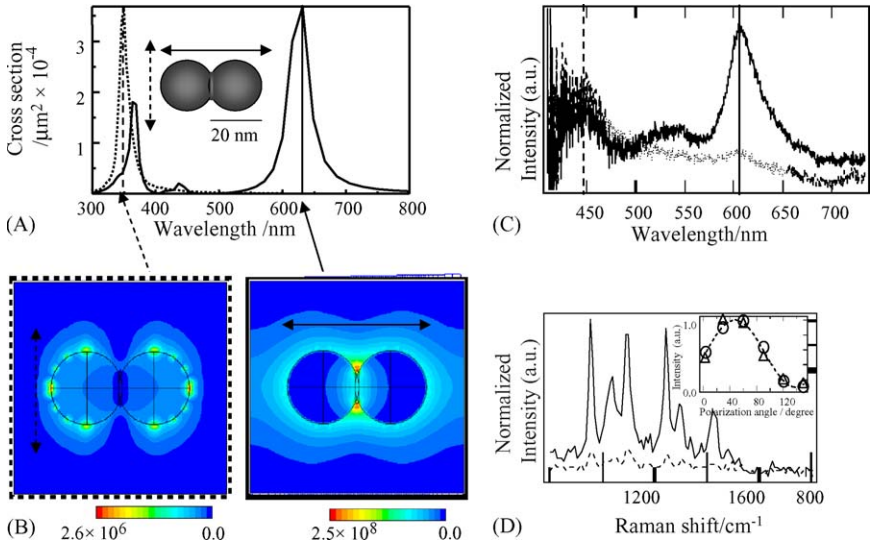

Fig. 3. (A) Calculated Rayleigh scattering spectra of an Ag nanoaggregate shown in the inset: solid and dotted curves are spectra with excitation polarization parallel to and perpendicular to long axis of the Ag nanoaggregate, respectively. (B) Calculated near-field images of the Ag nanoaggregate with excitation polarization perpendicular (left panel) to and parallel (right panel) to the long axis of the Ag nanoaggregate. Values of color scale are 4th power of ratios of incident EM field (E_{in}) and enhanced EM field (E_{loc}); $|E_{loc}/E_{in}|^4$. (C) Experimental Rayleigh scattering spectra of a Ag nanoaggregate with orthogonal excitation polarizations. (D) Experimental SERRS spectra corresponding to (C) with orthogonal excitation polarizations. Polarization angles are the same for solid curves in (C) and (D) and dotted curves in (C) and (D). Inset of (D): Intensity of the plasmon resonance maxima at 610 nm in (C) (open circles) and SERRS maxima in (D) (open squares) vs. polarization angles.

curve (data not shown). Therefore, this resonance band is likely a dipole. Also, we confirmed that polarization-angle dependence of near-field intensity at the NP junction was fitted with the same $\cos^2\theta$ curve (data not shown) as in the case of the plasmon resonance at 630 nm. The common $\cos^2\theta$ curve revealed that the enhanced near-field at NP junction was contributed by dipole of plasmon resonance with maximum at 630 nm.

Typical Rayleigh scattering spectra from a SERRS-active Ag nanoaggregate are shown in Fig. 3C. Rayleigh scattering spectra indicated by solid and dotted curves correspond to orthogonal excitation polarization angles. Interestingly, for a given excitation polarization the experimental (Fig. 3C) and calculated (Fig. 3A) curves showed only one major plasmon resonance band; band positions were not exactly the same though. Generally, the plasmon resonance maximums at 610, 530, and 445 nm in the experimental spectrum (Fig. 3C, solid curve) are comparable to the plasmon resonance maximums at 630, 440, and 360 nm in the calculated spectrum (Fig. 3A, solid curve). Furthermore, the polarization-angle dependence of the plasmon resonance maximums at 610 and 530 nm (inset of Fig. 3D) and 630 and 440 nm (data not shown) was also fitted with a common $\cos^2(\theta)$ curve; the $\cos^2(\theta)$ curve revealed that the plasmons are dipoles. From the identical spectral shapes and polarization dependence of the calculated and experimental plasmon resonance bands, we consider that the experimental maximum at 610 and 530 nm (Fig. 3C) corresponds to the calculated maximum at 630 and 440 nm (Fig. 3A), which is a longitudinal plasmons parallel to the long axis of a Ag nanoaggregate.

We have examined polarization-angle dependence of SERRS signals from identical Ag nanoaggregates and identified that the polarization-angle dependence of SERRS is similar to that of the plasmon resonance maximum at 610 nm (Fig. 3C). The SERRS signal detected from a single-Ag nanoaggregate showed maximum (solid curve in Fig. 3D) and minimum (dotted curve in Fig. 3D) intensities when the excitation polarization was parallel and perpendicular to the plasmon resonance band, respectively. The polarization-angle dependence of the SERRS intensity is shown in the inset of Fig. 3D. The polarization-angle dependence of both the plasmon and SERRS signals were fitted with a common $\cos^2(\theta)$ curve. This fitting strongly supports that the SERRS was contributed by an enhanced EM filed that was coupled to the plasmon resonance at 610 nm. From this relation between SERRS and plasmon resonance we consider that the SERRS intensity becomes optimum when the excitation polarization angle is parallel to the longitudinal plasmon mode in Rayleigh scattering spectrum.

3.2. Optimization of excitation wavelength for SERRS

Recently, excitation-wavelength dependence of SERRS was examined by using arrays of Au NPs with a homogeneous plasmon resonance band and identified that the wavelength of the plasmon resonance maxima affected the excitation-wavelength dependence of SERRS [19]. Here, we have identified optimum excitation-wavelength for SERRS on the basis of relations between excitation-wavelength dependence of SERRS and wavelength of plasmon resonance maxima of single-Ag nanoaggregates. For this, we have selected four single SERRS-active Ag nanoaggregates with different plasmon resonance maximums and examined relations between excitation-wavelength dependence of SERRS and plasmon resonance wavelength of individual nanoaggregates. From polarization dependence (results not shown) of these plasmon resonance maxima and SERRS maxima we confirmed that the plasmon dipoles were cou-

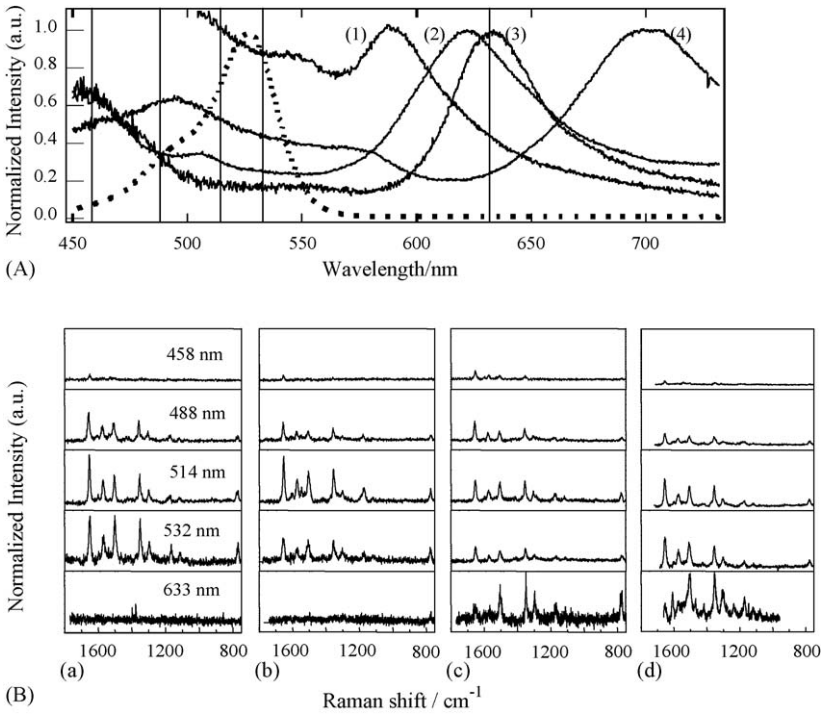

Fig. 4. (A) Solid curves (1–4): plasmon resonance Rayleigh scattering spectra of four single-Ag nanoaggregates; dashed curve: absorption spectrum of R6G. The vertical solid lines correspond to excitation laser wavelengths (458, 488, 514, 532, and 633 nm). (B) Panels (a–d) SERRS spectra of four SERRS-active single-Ag nanoaggregates measured by exciting at different wavelengths. The SERRS bands in (B) [panels (a–d)] correspond to plasmon resonance bands in (A) (1–4).

pled to SERRS, and we have directly investigated relationships between SERRS and plasmon resonance without considering inhomogenity caused by overlapping of many dipoles and multipoles in Ag nanoaggregates. Plasmon resonance bands selected from four Ag nanoaggregates with intensity maximums at 587, 622, 634, and 700 nm are shown in Fig. 4A (solid curves). The excitation laser wavelengths used were 458, 488, 514, 532, and 633 nm and are indicated by vertical lines in Fig. 4A. The dotted curve in Fig. 4A is the absorption spectrum of R6G. The excitation-wavelength dependences of SERRS signals from four Ag nanoaggregates are shown in Fig. 4B. Plasmon resonance of the nanoaggregates corresponding to the SERRS panels a–d are curves 1–4 in Fig. 4A.

It has been known that for a colloidal solution of SERRS-active Ag nanoaggregates the spectral shape of excitation-wavelength dependence of SERRS intensity is similar to absorption spectrum of R6G [16]. In particular, an aqueous solution of R6G has both the optical absorption maximum and the spectral shape of excitation-wavelength dependence of SERRS intensity around 525 nm [16]. Indeed, from single nanoaggregate SERRS investigations we have identified that a definitive similarity between absorption spectrum and excitation-wavelength dependency of SERRS is not valid from nanoaggregate to nanoaggregate. Typical example is shown in Fig. 4B [panels (a) and (b)] where under 633 nm excitation characteristic SERRS bands were absent for two nanoaggregates with higher energy plasmon resonance bands. On the other hand, under the same excitation conditions characteristic SERRS bands of R6G were clearly identified for other two nanoaggregates with relatively low plasmon resonance energy [panels (c) and (d)]. This comparison of the excitation-wavelength dependence and plasmon resonance bands suggested that excitation-wavelength for efficient SERRS shifts to the longer wavelength region as plasmon resonance maximum shifts to the longer wavelength region. The red-shifted excitation-wavelength likely shifted the EM field towards longer wavelength which produced the plasmon resonance. It may be noted that the excitation-wavelength for efficient SERRS is different from the plasmon resonance maximum as shown in Fig. 4B. For example; panel (b) in Fig. 4B shows that SERRS intensity was maximized when excited at 514 nm; although, the corresponding plasmon resonance maximum is at 622 nm. These observations suggested that ideal excitation-wavelength for SERRS is not always determined by molecular absorption maximum or plasmon resonance maximum but by spectral overlap between electronic absorption spectrum of a molecule and spectrum of EM filed intensity which is enhanced by coupling between particle plasmon and incident laser light. In general, we consider that optimum excitation-wavelength for SERRS is between a plasmon resonance maximum and a molecular absorption maximum.

3.3. Plasmon resonance maxima and SERRS

SERRS spectra differ from normal Raman spectra and also differs each other from nanoaggregate to nanoaggregate [10,16,17]. These differences provided difficulties in characterizing molecules by SERRS analyses. The origin of the differences has been attributed to variations in chemical interaction between adsorbed molecules and surface metal atoms [10,16,17]

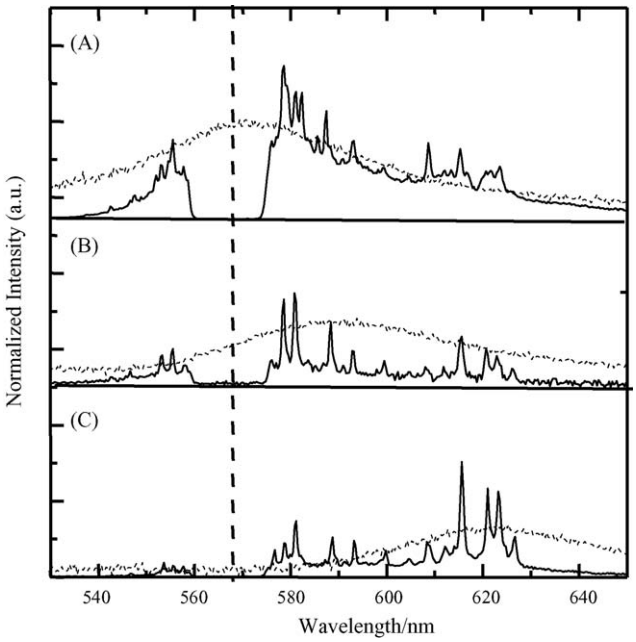

Fig. 5. Plasmon resonance maxima dependence of SERRS spectra from three Ag nanoaggregates. Plasmon resonance Rayleigh scattering spectra are indicated by dotted curves and SERRS spectra by solid curves.

or temperature variations of SERRS-active molecule [18]. We have investigated the contribution of plasmon resonance maxima to the above differences. In this investigation we have considered that SERRS spectra are varied by plasmon resonance band shape because SERRS EM model predicts that SERRS photon radiation is mediated by plasmon dipole radiation [2–4].

In order to explore the origin of the plasmon-resonance dependence of spectral-variations in SERRS, we have measured SERRS of Rhodamine 123 and plasmon resonance bands of three Ag nanoaggregates. Typical plasmon resonance bands (dotted curve) and SERRS bands (solid curves) from three Ag nanoaggregates obtained under 568-nm laser excitation are shown in Fig. 5. Interestingly, the SERRS bands near the plasmon resonance maximum were selectively enhanced. The selective enhancement of SERRS bands are presented in Fig. 5A–C. Fig. 5A shows that a plasmon resonance maximum at 570 nm and SERRS bands around 570 nm, which corresponds to Raman shift of 400 cm^{-1}, are larger than other SERRS bands. Fig. 5B shows that a plasmon resonance maximum at 590 nm and SERRS bands around 570 and 620 nm are equally enhanced. Fig. 5C shows that a plasmon resonance maximum at 620 nm and SERRS bands around 620 nm, which corresponds to a Raman shift of 1500 cm^{-1}, are larger than other SERRS bands. The observed selective enhancement of SERRS bands is consistent with SERRS EM model [2–4], which pointed out SERRS as a two-fold enhanced Raman scattering; first, enhancement from incident light, and second, enhancement from scattered light. The second enhancement is rephrased as radiation of Raman scattering photon is mediated by plasmon dipole radiation. Thus, we consider that SERRS spectral envelop is modulated by spectral envelop of plasmon resonance Rayleigh scattering. Therefore, the observed spectral modulation of SERRS dictates a consideration that a SERRS spectrum is a convolution between normal Raman spectrum and plasmon resonance Rayleigh scattering spectrum.

4. Conclusions

We developed a dark-field microspectroscopic system by combining Rayleigh scattering spectroscopy and SERRS spectroscopy on an optical microscope, and this system enabled us to investigate simultaneously plasmon resonance Rayleigh scattering and SERRS of single-Ag nanoaggregates. Our investigations directly demonstrated three kinds of relationships between plasmon resonance and SERRS. From these investigations we have identified relationships among excitation polarization, excitation energy, and plasmon resonance energy, and we arrived at three specific conclusions: (1) SERRS bands have the same polarization dependence as that of a longitudinal mode plasmon resonance band, suggesting that excitation polarization set parallel to the longitudinal plasmon mode can provide maximum SERRS intensity; (2) SERRS intensity is dependent on plasmon resonance maximum, suggesting that larger overlap between molecular absorption band and plasmon resonance band can provide higher SERRS intensity; (3) spectral shape of SERRS is reliant on plasmon resonance energy, suggesting that SERRS spectrum can be modulated by plasmon resonance band shape.

Acknowledgements

This study was partly supported by Grant-in-Aid for Young Scientists “WAKATE (B)” (no. 16760042) from The Ministry of Education, Culture, Sports and Science and Technology (MEXT) of Japan. This work was also supported by “Open Research Center” project for private universities: matching fund subsidy from MEXT.

References

[1] (a) U. Kreibig, M. Vollmer, Optical Properties of Metal Clusters, vol. 25. Springer Series in Materials Science, Springer, Berlin, 1995;
(b) F. Bohren, D.R. Huffman, Absorption and Scattering of Light by Small Particles, Wiley, New York, 1983;
(c) J.J. Mock, M. Barbic, D.R. Smith, D.A. Schultz, S. Schultz, J. Chem. Phys. 116 (2002) 6755.
[2] M. Moskovits, Rev. Mod. Phys. 57 (1985) 783.
[3] F.J. Garcıĭa-Vidal, J.B. Pendry, Phys. Rev. Lett. 77 (1996) 1163.
[4] H. Xu, E.J. Bjerneld, M. Käll, L. Börjesson, Phys. Rev. Lett. 83 (1999) 4357.
[5] M. Futamata, Y. Maruyama, M. Ishikawa, Vib. Spectrosc. 30 (2002) 1714.
[6] E. Hao, G.C. Schatz, J. Chem. Phys. 120 (2004) 357.
[7] M. Kawasaki, S. Mine, J. Phys. Chem. B 109 (2005) 17254.
[8] T. Itoh, K. Hashimoto, A. Ikehata, Y. Ozaki, Appl. Phys. Lett. 83 (2003) 5557.
[9] (a) G. Bauer, J. Hassmann, H. Walter, J. Haglmuller, C. Mayer, T. Schalkhammer, Nanotechnology 14 (2003) 1289;
(b) A. Ikehata, T. Itoh, Y. Ozaki, Anal. Chem. 76 (2004) 6461.
[10] A. Otto, I. Mrozek, H. Grabhorn, W. Akemann, J. Phys. Condens. Matter 4 (1992) 1143.
[11] K. Kneipp, Y. Wang, H. Kneipp, L.T. Perelman, I. Itzkan, R.R. Dasari, M.S. Feld, Phys. Rev. Lett. 78 (1997) 1667.
[12] S. Nie, S.R. Emory, Science 275 (1997) 1102.

[13] A.M. Michaels, M. Nirmal, L.E. Brus, J. Am. Chem. Soc. 121 (1999) 9932.
[14] (a) T. Itoh, K. Hashimoto, Y. Ozaki, Appl. Phys. Lett. 83 (2003) 2274;
(b) T. Itoh, V. Biju, M. Ishikawa, Y. Kikkawa, K. Hashimoto, A. Ikehata, Y. and, Ozaki, J. Chem. Phys. 124 (2006) 134708.
[15] T. Itoh, K. Hashimoto, A. Ikehata, Y. Ozaki, Chem. Phys. Lett. 389 (2004) 225.
[16] P. Hildebrant, M. Stockburger, J. Phys. Chem. 88 (1984) 5935.
[17] A. Weiss, G. Haran, J. Phys. Chem. B 105 (2001) 12348.
[18] Y. Maruyama, M. Ishikawa, M. Futamata, J. Phys. Chem. B 108 (2004) 673.
[19] A.D. McFarland, M.A. Young, J.A. Dieringer, R.P. Van Duyne, J. Phys. Chem. B. 109 (2005) 11279.
[20] (a) T. Itoh, Y. Ozaki, H. Yoshikawa, T. Ihama, H. Masuhara, Appl. Phys. Lett. 88 (2006) 084102;
(b) G. Brehm, G. Sauer, N. Fritz, S. Schneider, S. Zaitsev, J. Mol. Struct. 735 (2005) 85;
(c) L.A. Lipscomb, S. Nie, S. Feng, N.-T. Yu, Chem. Phys. Lett. 170 (1990) 457;
(d) K. Kneipp, H. Kneipp, I. Itzkan, R.R. Dasari, M.S. Feld, Chem. Phys. 247 (1999) 155.
[21] T. Itoh, K. Hashimoto, V. Biju, M. Ishikawa, Y. Ozaki, J. Phys. Chem. B 110 (2006) 9579.
[22] P.C. Lee, D.J. Meisel, Phys. Chem. 86 (1982) 3391.
[23] T. Itoh, T. Asahi, H. Masuhara, Appl. Phys. Lett. 79 (2001) 1667.